

# Coupled three-mode squeezed vacuum: Gaussian steering and Remote generation of Wigner negativity

Zi-wei Zhan, Bo Lan, Jian Wang and Xue-xiang Xu<sup>†</sup>  
College of Physics and Communication Electronics,  
Jiangxi Normal University, Nanchang 330022, China;  
<sup>†</sup>xuxuexiang@jxnu.edu.cn

Coupled three-mode squeezed vacuum (C3MSV), as a typical (and pure) three-mode Gaussian state, will become an useful entangled resource in future quantum protocols because of its potential attributes. In this paper, we analyze all bipartite Gaussian steerings (including no steering, one-way steering and two-way steering) present in different modes of the C3MSV. Through the steerings shared in the C3MSV, we propose schemes of remotely generating Wigner negativity by performing appropriate photon subtraction(s) in the local position.

**Keywords:** Gaussian steering; Wigner negativity

## I. INTRODUCTION

In many previous quantum protocols, Einstein-Podolsky-Rosen (EPR) state is perhaps the most commonly used entangled resource[1]. Some other entangled resources, such as NOON state[2, 3] and Greenberger-Horne-Zeilinger (GHZ) state[4], have also been used in other different situations. With the development and requirements of technology, more and more entangled resources are introduced and used in various protocols[5–9]. In current technology, there is a tread for researchers to use multi-mode or multi-partite resources. Recently, Zhang and Glasser[10] introduced the coupled three-mode squeezed vacuum (C3MSV), which arises our research interest. Intuitively, we think that the C3MSV will become an useful entangled resource in future quantum protocols. Except those properties such as squeezing and entanglement considered by Zhang and Glasser, we will further study other properties for the C3MSV in this paper.

Quantum correlations, which is established as a powerful resource in two-party, three-party or even more-party systems, have been intensively investigated in recent years and can manifest in different forms, such as entanglement, steering and Bell nonlocality[11]. Entanglement is a striking feature of describing the non-biseparability of states for two or more parties[12]. Bell nonlocality offers a vast research landscape with relevance for fundamental[13] and quantum technological applications[14, 15]. Eistein-Podolsky-Rosen (EPR) steering is intermediate between entanglement and Bell nonlocality[16–20]. Generally, steerable states are a strict subset of the entangled states and a strict superset of states that exhibit Bell nonlocality[21, 22]. All these correlations can be used as resources for quantum enhanced tasks[23–26]. On the other hand, Wigner negativity (WN)[27] is arguably one of the most striking non-classical features of quantum states[28]. Beyond its fundamental relevance[29, 30], it is also a necessary resource for quantum speedup with continuous variables. For example, WN has been seen as a necessary ingredient in CV quantum computation and simulation to out-

perform classical devices[31, 32].

As two important signatures of nonclassicality, quantum correlations can be intertwined with Wigner negativity in the conditional generation of non-Gaussian states[33, 34]. Walschaers et al. developed a general formalism to prepare Wigner-negative states through EPR steering[35–37]. Recently, Xiang et al. proposed schemes for remote generation of Wigner negativity through EPR steering in multipartite scenario[38], where they used a pure three-mode Gaussian state (realized by a feasible linear optical network) as resource. Following that work, we shall use the C3MSV as entangled resource to prepare Wigner negative states in this work.

The rest of the paper is structured as follows: In section 2, we make a brief introduction of the coupled three-mode squeezing operator (C3MSO) and the coupled three-mode squeezed vacuum (C3MSV). In Section 3, we investigate the bipartite Gaussian steerings in the C3MSV. In section 4, we propose schemes to remotely generate Wigner negativity based on the steering in the C3MSV. Conclusions are summarized in the last section.

## II. COUPLED THREE-MODE SQUEEZED VACUUM

In nonlinear and quantum optics, there are a number of nonlinear optical processes to realize various squeezing or multipartite entanglement[39, 40]. In this section, we make a brief introduction of the C3MSO and the C3MSV[10]. The C3MSO  $S_3(\xi_1, \xi_2)$  is expressed as the following compact form

$$S_3 = e^{\xi_1^\dagger a_1 a_2 + \xi_2^\dagger a_2 a_3 - \xi_1 a_1^\dagger a_2^\dagger - \xi_2 a_2^\dagger a_3^\dagger}, \quad (1)$$

where  $\xi_j = r_j e^{i\theta_j}$  ( $j = 1, 2$ ) are the two complex squeezing parameters, with respective magnitude  $r_j$  and phase  $\theta_j$ . It is obvious to see  $S_3^{-1} = S_3^\dagger$ . For the convenience purpose, we reset  $(r_1, r_2)$  as  $(r, \phi)$ , satisfying  $r = \sqrt{r_1^2 + r_2^2}$ , and  $\cos \phi = r_1/r$ ,  $\sin \phi = r_2/r$  with  $\phi \in [0, \pi/2]$  (see Fig.1(a)).

As shown in Fig.1(b), we further operate  $S_3$  on

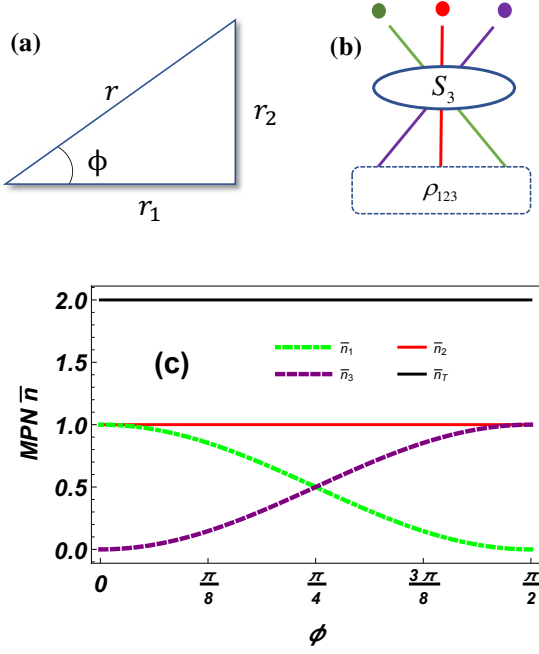


FIG. 1: (a)  $(r_1, r_2)$  are reset to  $(r, \phi)$ ; (b) Conceptual generating scheme of the C3MSV; (c) MPNs  $\bar{n}_1, \bar{n}_2, \bar{n}_3$  and  $\bar{n}_T$  versus  $\phi$  (setting  $\bar{n}_T = 2$ ).

$|0\rangle|0\rangle|0\rangle$  and obtain the C3MSV

$$|\psi\rangle \equiv S_3 |000\rangle = \frac{1}{c} e^{-\frac{\epsilon_1}{c} a_1^\dagger a_2^\dagger - \frac{\epsilon_2}{c} a_2^\dagger a_3^\dagger} |000\rangle, \quad (2)$$

whose density operator is  $\rho_{123} = |\psi\rangle\langle\psi|$ . Here, we set  $c = \cosh r$ ,  $s = \sinh r$ ,  $\epsilon_1 = s e^{i\theta_1} \cos \phi$ , and  $\epsilon_2 = s e^{i\theta_2} \sin \phi$ . In particular, if  $\xi_2 = 0$ , then  $|\psi\rangle = S_2(\xi_1) |00\rangle_{12} \otimes |0\rangle_3$ ; if  $\xi_1 = 0$ , then  $|\psi\rangle = |0\rangle_1 \otimes S_2(\xi_2) |00\rangle_{23}$ , with  $S_2(\xi_1) = e^{\xi_1^* a_1 a_2 - \xi_1 a_1^\dagger a_2^\dagger}$  and  $S_2(\xi_2) = e^{\xi_2^* a_2 a_3 - \xi_2 a_2^\dagger a_3^\dagger}$ . Moreover, if  $\xi_1 = \xi_2$  (i.e.  $\phi = \pi/4$ ), the C3MSV is a bisymmetric state, whose mode-1 and mode-3 are symmetrical with mode-2.

Using Eq.(A.4), we easily obtain  $\bar{n}_1 = s^2 \cos^2 \phi$ ,  $\bar{n}_2 = s^2$ ,  $\bar{n}_3 = s^2 \sin^2 \phi$  and  $\bar{n}_T = 2s^2$ , i.e., the mean photon numbers (MPNs) for mode-1, mode-2, mode-3 and total modes, respectively (see Fig.1(c)). By the way, we often replace  $r$  by  $\bar{n}_T$  (using  $r = \text{arcsinh} \sqrt{\bar{n}_T/2}$ ) and set  $\theta_1 = \theta_2 = 0$  in our numerical works.

### III. GAUSSIAN STEERING IN THE C3MSV

The C3MSV is a pure three-mode entangled Gaussian state, which can be seen from its Wigner function provided in Eq.(B.0). In this section, we focus on analyzing the distributions of bipartite Gaussian steerings in the C3MSV.

#### A. Covariance Matrix of the C3MSV

The covariance matrix (CM)[41–45] of the C3MSV is expressed as

$$V = \begin{pmatrix} (1 + 2\bar{n}_1) 1_2 & -2sc \cos \phi \Sigma_{\theta_1} & s^2 \sin 2\phi R_{\theta_2 - \theta_1} \\ -2sc \cos \phi \Sigma_{\theta_1} & (1 + 2\bar{n}_2) 1_2 & -2sc \sin \phi \Sigma_{\theta_2} \\ s^2 \sin 2\phi R_{\theta_2 - \theta_1} & -2sc \sin \phi \Sigma_{\theta_2} & (1 + 2\bar{n}_3) 1_2 \end{pmatrix}, \quad (3)$$

with  $2 \times 2$  identity matrix  $1_2$  and

$$\Sigma_\theta = \begin{pmatrix} \cos \theta & \sin \theta \\ \sin \theta & -\cos \theta \end{pmatrix}, R_\theta = \begin{pmatrix} \cos \theta & \sin \theta \\ -\sin \theta & \cos \theta \end{pmatrix}. \quad (4)$$

The matrix elements of the CM, defined by  $V_{jk} = \langle \psi | (\hat{X}_j \hat{X}_k + \hat{X}_k \hat{X}_j) | \psi \rangle$ , are expressed via the vector  $\hat{X} = (\hat{x}_1, \hat{p}_1, \hat{x}_2, \hat{p}_2, \hat{x}_3, \hat{p}_3)$ . For each mode, we define position operator  $\hat{x}_j = \frac{1}{\sqrt{2}}(\hat{a}_j + \hat{a}_j^\dagger)$  and momentum operator  $\hat{p}_j = \frac{1}{i\sqrt{2}}(\hat{a}_j - \hat{a}_j^\dagger)$ , accompanying with its annihilation and creation operators  $\hat{a}_j, \hat{a}_j^\dagger$ . It is noted that  $\langle \hat{x}_j \rangle = \langle \hat{p}_j \rangle = 0$  for each mode of the C3MSV. The CM  $V$  in Eq.(3) is a symmetric and positive semidefinite matrix (with eigenvalues  $1, 1, e^{-2r}, e^{-2r}, e^{2r}, e^{2r}$ ) and obeys  $V + i\Omega^{\oplus 3} \geq 0$  with  $\Omega = \begin{pmatrix} 0 & 1 \\ -1 & 0 \end{pmatrix}$ . Moreover, we can check  $\det V = 1$  and prove that the C3MSV is a pure state.

#### B. Bipartite Gaussian steering

Gaussian steering is a steering by Gaussian measurements[46, 47]. Reid derived monogamy inequalities for the bipartite EPR steering distributed among different systems[48]. Xiang et al. derived the laws for the distribution of quantum steering among different parties and prove a monogamy relation of Gaussian steering[49]. Here, we make a brief review for Gaussian steering.

The CM of a bipartite Gaussian state can be expressed as

$$\sigma_{AB} = \begin{pmatrix} V_A & V_{AB} \\ V_{AB}^T & V_B \end{pmatrix}, \quad (5)$$

where party  $A$  and party  $B$  are the bipartite subsystems. Then, we can quantify how much it is steerable via the following quantity

$$\mathcal{G}^{A \rightarrow B}(V) := \max\{0, -\sum_{j: \bar{v}_j^{B|A} < 1} \ln \bar{v}_j^{B|A}\}. \quad (6)$$

where  $\{\bar{v}_j^{B|A}\}_{j=1}^{2n_B}$  denote the symplectic eigenvalues ( $n_B$  is the mode number in subsystem  $B$ ) of the Schur complement  $\sigma_{B|A} = V_B - V_{AB}^T V_A^{-1} V_{AB}$  of  $\sigma_{AB}$ . This quantity  $\mathcal{G}^{A \rightarrow B}$  is defined as Gaussian  $A \rightarrow B$  steerability, which

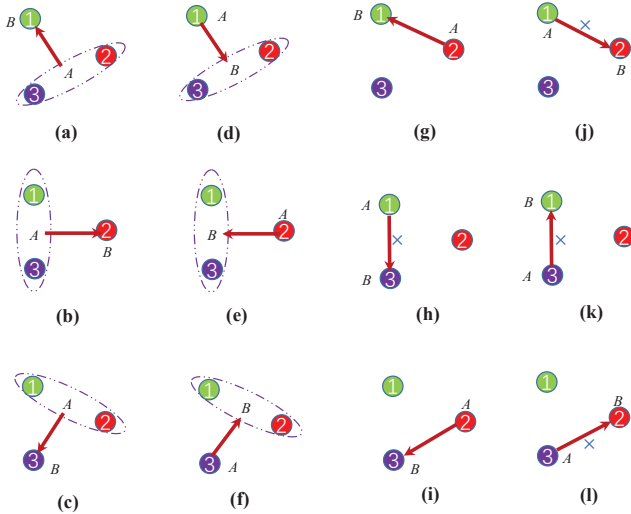


FIG. 2: Bipartite assignments in the C3MSV, where A is the steering party and B is the steered party.

is a monotone under Gaussian local operations and classical communication. Moreover, the larger  $\mathcal{G}^{A \rightarrow B}$  is, the stronger Gaussian steerability is [50, 51].

In what follows, we take party A and party B from the three modes of the C3MSV and construct 12 kinds of  $\sigma_{ABs}$  from  $V$  in Eq.(3). The steering party A and the steered party B are assigned as shown in Fig.2. According to the rule in Eq.(6), we obtain the following steerings present in the C3MSV.

*Case (a)  $\Rightarrow$  A(23)-B(1):* In this case, we have  $\bar{\nu}_1^{B|A} = \bar{\nu}_2^{B|A} = (c^2 + s^2 \cos 2\phi)^{-1} < 1$ , which leads to

$$\mathcal{G}^{23 \rightarrow 1} = 2 \ln(c^2 + s^2 \cos 2\phi). \quad (7)$$

*Case (b)  $\Rightarrow$  A(13)-B(2):* In this case, we obtain two eigen  $\bar{\nu}_1^{B|A} = \bar{\nu}_2^{B|A} = (c^2 + s^2)^{-1} < 1$ , which leads to

$$\mathcal{G}^{13 \rightarrow 2} = 2 \ln(c^2 + s^2). \quad (8)$$

*Case (c)  $\Rightarrow$  A(12)-B(3):* In this case, we have  $\bar{\nu}_1^{B|A} = \bar{\nu}_2^{B|A} = (c^2 - s^2 \cos 2\phi)^{-1} < 1$ , which leads to

$$\mathcal{G}^{12 \rightarrow 3} = 2 \ln(c^2 - s^2 \cos 2\phi). \quad (9)$$

*Case (d)  $\Rightarrow$  A(1)-B(23):* In this case, we have  $\bar{\nu}_1^{B|A} = \bar{\nu}_2^{B|A} = (\varkappa_1 - \sqrt{\varkappa_2})/\varkappa_0 < 1$  and  $\bar{\nu}_3^{B|A} = \bar{\nu}_4^{B|A} = (\varkappa_1 + \sqrt{\varkappa_2})/\varkappa_0 \geq 1$ , which leads to

$$\mathcal{G}^{1 \rightarrow 23} = 2 \ln[\varkappa_0 / (\varkappa_1 - \sqrt{\varkappa_2})], \quad (10)$$

with

$$\begin{aligned} \varkappa_0 &= 4 + 8s^2 \cos^2 \phi, \\ \varkappa_1 &= 1 + 3c^2 + (3 - 2 \cos 2\phi) s^2, \\ \varkappa_2 &= (19 - 12 \cos 2\phi) c^2 s^2 \\ &\quad + (19 - 12 \cos 2\phi + 2 \cos 4\phi) s^4 \\ &\quad + (13 - 20 \cos 2\phi) s^2. \end{aligned} \quad (11)$$

*Case (e)  $\Rightarrow$  A(2)-B(13):* In this case, we have  $\bar{\nu}_1^{B|A} = \bar{\nu}_2^{B|A} = (c^2 + s^2)^{-1} < 1$  and  $\bar{\nu}_3^{B|A} = \bar{\nu}_4^{B|A} = 1$ , which leads to

$$\mathcal{G}^{2 \rightarrow 13} = 2 \ln(c^2 + s^2). \quad (12)$$

*Case (f)  $\Rightarrow$  A(3)-B(12):* In this case, we have  $\bar{\nu}_1^{B|A} = \bar{\nu}_2^{B|A} = (\iota_1 - \sqrt{\iota_2})/\iota_0 < 1$  and  $\bar{\nu}_3^{B|A} = \bar{\nu}_4^{B|A} = (\iota_1 + \sqrt{\iota_2})/\iota_0 \geq 1$ , which leads to

$$\mathcal{G}^{3 \rightarrow 12} = 2 \ln[\iota_0 / (\iota_1 - \sqrt{\iota_2})], \quad (13)$$

with

$$\begin{aligned} \iota_0 &= 4 + 8s^2 \sin^2 \phi, \\ \iota_1 &= 1 + 3c^2 + (3 + 2 \cos 2\phi) s^2, \\ \iota_2 &= (19 + 12 \cos 2\phi) c^2 s^2 + \\ &\quad (19 + 12 \cos 2\phi + 2 \cos 4\phi) s^4 \\ &\quad + (13 + 20 \cos 2\phi) s^2. \end{aligned} \quad (14)$$

*Case (g)  $\Rightarrow$  A(2)-B(1):* In this case, we have  $\bar{\nu}_1^{B|A} = \bar{\nu}_2^{B|A} = (c^2 - s^2 \cos 2\phi)/(c^2 + s^2) < 1$ , which leads to

$$\mathcal{G}^{2 \rightarrow 1} = 2 \ln[(c^2 + s^2)/(c^2 - s^2 \cos 2\phi)]. \quad (15)$$

*Case (h)  $\Rightarrow$  A(1)-B(3):* In this case, we have  $\bar{\nu}_1^{B|A} = \bar{\nu}_2^{B|A} = (c^2 + s^2)/(1 + 2s^2 \cos^2 \phi) \geq 1$ , which leads to

$$\mathcal{G}^{1 \rightarrow 3} = 0. \quad (16)$$

*Case (i)  $\Rightarrow$  A(2)-B(3):* In this case, we have  $\bar{\nu}_1^{B|A} = \bar{\nu}_2^{B|A} = (c^2 + s^2 \cos 2\phi)/(c^2 + s^2) < 1$ , which leads to

$$\mathcal{G}^{2 \rightarrow 3} = 2 \ln[(c^2 + s^2)/(c^2 + s^2 \cos 2\phi)]. \quad (17)$$

*Case (j)  $\Rightarrow$  A(1)-B(2):* In this case, we have  $\bar{\nu}_1^{B|A} = \bar{\nu}_2^{B|A} = (c^2 - s^2 \cos 2\phi)/(1 + 2s^2 \cos^2 \phi) \geq 1$ , which leads to

$$\mathcal{G}^{1 \rightarrow 2} = 0. \quad (18)$$

*Case (k)  $\Rightarrow$  A(3)-B(1):* In this case, we have  $\bar{\nu}_1^{B|A} = \bar{\nu}_2^{B|A} = (c^2 + s^2)/(1 + 2s^2 \sin^2 \phi) \geq 1$ , which leads to

$$\mathcal{G}^{3 \rightarrow 1} = 0. \quad (19)$$

*Case (l)  $\Rightarrow$  A(3)-B(2):* In this case, we have  $\bar{\nu}_1^{B|A} = \bar{\nu}_2^{B|A} = (c^2 + s^2 \cos 2\phi)/(1 + 2s^2 \sin^2 \phi) \geq 1$ , which leads to

$$\mathcal{G}^{3 \rightarrow 2} = 0. \quad (20)$$

It is necessary to notice that all above steerings are independent of phases  $(\theta_1, \theta_2)$ . In Fig.3, we draw the contour plots of  $\mathcal{G}^{12 \rightarrow 3}$ ,  $\mathcal{G}^{1 \rightarrow 23}$ ,  $\mathcal{G}^{23 \rightarrow 1}$ ,  $\mathcal{G}^{3 \rightarrow 12}$ ,  $\mathcal{G}^{2 \rightarrow 1}$  and  $\mathcal{G}^{2 \rightarrow 3}$  in the  $(\bar{n}_T, \phi)$ -space. In Fig.4, we plot  $\mathcal{G}^{A \rightarrow Bs}$

versus  $\phi$  (with  $\bar{n}_T = 3$ ) and  $\mathcal{G}^{A \rightarrow B}$ s versus  $\bar{n}_T$  (with  $\phi = \pi/8$ ). Among them,  $\mathcal{G}^{13 \rightarrow 2} = \mathcal{G}^{2 \rightarrow 13}$  are functions of  $\bar{n}_T$  and are not independent of  $\phi$ . Moreover, we know that  $\mathcal{G}^{1 \rightarrow 2} = \mathcal{G}^{1 \rightarrow 3} = \mathcal{G}^{3 \rightarrow 1} = \mathcal{G}^{3 \rightarrow 2} = 0$ , but  $\mathcal{G}^{2 \rightarrow 1} > 0$  (except  $\phi = \pi/2$ ),  $\mathcal{G}^{2 \rightarrow 3} > 0$  (except  $\phi = 0$ ) and  $\mathcal{G}^{2 \rightarrow 1} = \mathcal{G}^{2 \rightarrow 3}$  for  $\phi = \pi/4$ . These results tell us that three types of steerings, i.e., no steering ( $A$  cannot steer  $B$  and  $B$  cannot steer  $A$ ), one-way steering ( $A$  can steer  $B$  while  $B$  cannot steer  $A$ ), or two-way (symmetrical or asymmetrical) steering ( $A$  can steer  $B$  and  $B$  can steer  $A$ ), are presented in the C3MSV. Main results are summarized as:

(i) There is no steering between mode 1 and mode 3 because of  $\mathcal{G}^{1 \rightarrow 3} = 0$  and  $\mathcal{G}^{3 \rightarrow 1} = 0$ , see Eq.(16) and Eq.(19);

(ii) There is one-way steering between mode 1 and mode 2 because of  $\mathcal{G}^{2 \rightarrow 1} > 0$  and  $\mathcal{G}^{1 \rightarrow 2} = 0$ , see Eq.(15) and Eq.(18);

(iii) There is one-way steering between mode 2 and mode 3 because of  $\mathcal{G}^{2 \rightarrow 3} > 0$  and  $\mathcal{G}^{3 \rightarrow 2} = 0$ , see Eq.(17) and Eq.(20);

(iv) There is two-way asymmetrical steering between mode 1 and modes 23 because of  $\mathcal{G}^{23 \rightarrow 1} > 0$  and  $\mathcal{G}^{1 \rightarrow 23} > 0$  but  $\mathcal{G}^{23 \rightarrow 1} \neq \mathcal{G}^{1 \rightarrow 23}$ , see Eq.(7) and Eq.(10);

(v) There is two-way symmetrical steering between mode 2 and modes 13 because of  $\mathcal{G}^{13 \rightarrow 2} = \mathcal{G}^{2 \rightarrow 13} > 0$ , see Eq.(8) and Eq.(12);

(vi) There is two-way asymmetrical steering between mode 3 and modes 12 because of  $\mathcal{G}^{12 \rightarrow 3} > 0$  and  $\mathcal{G}^{3 \rightarrow 12} > 0$  but  $\mathcal{G}^{12 \rightarrow 3} \neq \mathcal{G}^{3 \rightarrow 12}$ , see Eq.(9) and Eq.(13).

Just like what He et al. said in their work[20], our results also show that each mode can be steered by one or both of the other two in the C3MSV. Moreover, we find that (a)  $\mathcal{G}^{2 \rightarrow 1} > 0$ , but  $\mathcal{G}^{3 \rightarrow 1} = 0$  and (b)  $\mathcal{G}^{2 \rightarrow 3} > 0$ , but  $\mathcal{G}^{1 \rightarrow 3} = 0$ . This result holds the character that two parties cannot steer the same system[48].

### C. Monogamy relations

In 2017, Xiang et al. defined the concept of the residual Gaussian steering (RGS)[49]. Here, we shall use the RGS to quantify the genuine tripartite steering for the C3MSV. Using all above expressions from Eq.(7) to Eq.(20), we check that the monogamy relations

$$\begin{aligned} \mathcal{G}^{(23) \rightarrow 1} - \mathcal{G}^{2 \rightarrow 1} - \mathcal{G}^{3 \rightarrow 1} &\geq 0, \\ \mathcal{G}^{(31) \rightarrow 2} - \mathcal{G}^{3 \rightarrow 2} - \mathcal{G}^{1 \rightarrow 2} &\geq 0, \\ \mathcal{G}^{(12) \rightarrow 3} - \mathcal{G}^{1 \rightarrow 3} - \mathcal{G}^{2 \rightarrow 3} &\geq 0, \end{aligned} \quad (21)$$

and

$$\begin{aligned} \mathcal{G}^{1 \rightarrow (23)} - \mathcal{G}^{1 \rightarrow 2} - \mathcal{G}^{1 \rightarrow 3} &\geq 0, \\ \mathcal{G}^{2 \rightarrow (31)} - \mathcal{G}^{2 \rightarrow 3} - \mathcal{G}^{2 \rightarrow 1} &\geq 0, \\ \mathcal{G}^{3 \rightarrow (12)} - \mathcal{G}^{3 \rightarrow 1} - \mathcal{G}^{3 \rightarrow 2} &\geq 0, \end{aligned} \quad (22)$$

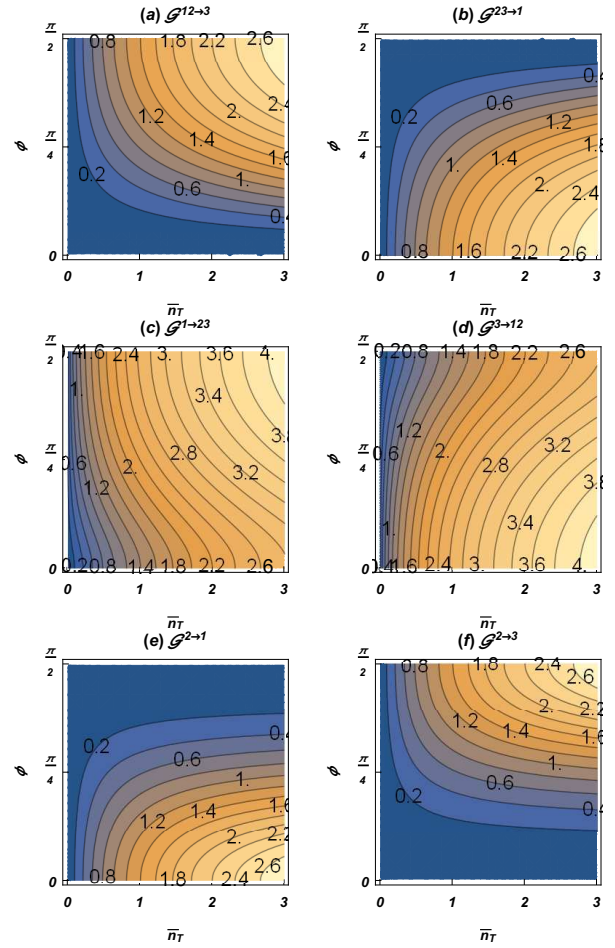


FIG. 3: (a)  $\mathcal{G}^{12 \rightarrow 3}$ , (b)  $\mathcal{G}^{23 \rightarrow 1}$ , (c)  $\mathcal{G}^{1 \rightarrow 23}$ , (d)  $\mathcal{G}^{3 \rightarrow 12}$ , (e)  $\mathcal{G}^{2 \rightarrow 1}$  and (f)  $\mathcal{G}^{2 \rightarrow 3}$  as functions of  $\bar{n}_T$  and  $\phi$ .

hold for the C3MSV. Further, we consider the RGS

$$\begin{aligned} \mathcal{G}^{1:2:3} &= \min_{\langle i,j,k \rangle} \{ \mathcal{G}^{(jk) \rightarrow i} - \mathcal{G}^{j \rightarrow i} - \mathcal{G}^{k \rightarrow i} \} \\ &= \min_{\langle i,j,k \rangle} \{ \mathcal{G}^{i \rightarrow (jk)} - \mathcal{G}^{i \rightarrow j} - \mathcal{G}^{i \rightarrow k} \}, \end{aligned} \quad (23)$$

for the C3MSV, where  $\langle i, j, k \rangle$  denotes any cycle permutation of 1, 2, 3. In Fig.5(a) we plot the RGS as a function of  $\bar{n}_T$  and  $\phi$ . From which, we see that the RGS is maximized on bisymmetric C3MSV with  $\phi = \pi/4$ , i.e.,  $r_1 = r_2$ . In this case, the genuine tripartite  $\mathcal{G}^{1:2:3}$  reduces to the collective steering  $\mathcal{G}^{13 \rightarrow 2} = \mathcal{G}^{2 \rightarrow 13} = 2 \ln(c^2 + s^2)$ . Figure 5(b) presents the RGS as a function of  $\phi$  with different  $\bar{n}_T$ , which are the sections of Fig.5(a). Indeed, the RGS acts as an indicator of collective steering-type correlations.

### IV. REMOTELY GENERATED WIGNER NEGATIVITY

As Walschaers recently pointed out, when party  $A$  and party  $B$  share a Gaussian state, party  $B$  can perform

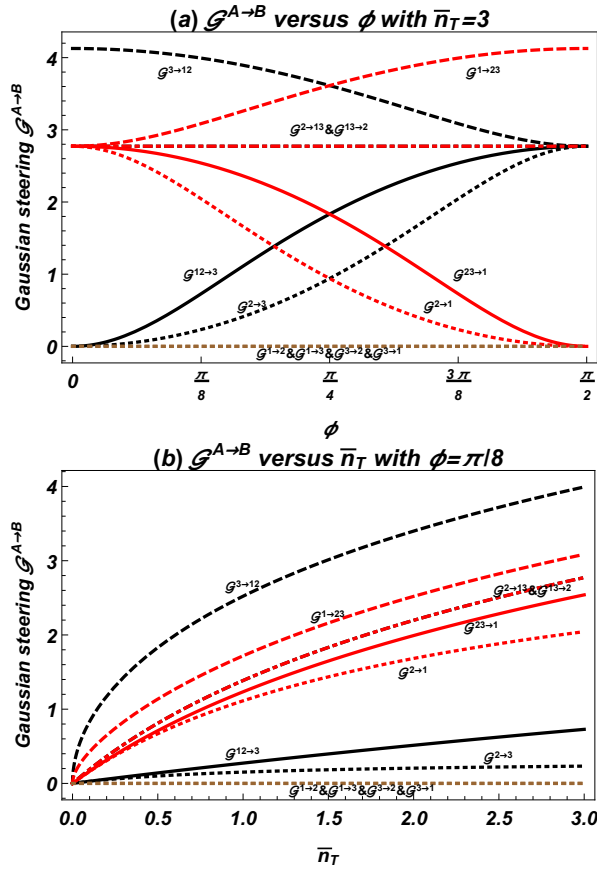


FIG. 4: (a)  $\mathcal{G}^{A \rightarrow B}$  versus  $\phi$  (setting  $\bar{n}_T = 3$ ); (b)  $\mathcal{G}^{A \rightarrow B}$  versus  $\bar{n}_T$  (setting  $\phi = \pi/8$ ).

some measurement on itself to create Wigner negativity on party  $A$ , if and only if there is a Gaussian steering from party  $A$  to party  $B$ [33]. Following ways in Xiang's work[38] and Walschaers' work[35], we investigate the remote creation and distribution of Wigner negativity (WN) in the tripartite C3MSV. Based on the C3MSV, we remain the steered party  $B$  in the local station and sent the steering party  $A$  to the remote position. After appropriate single-photon subtraction(s) on the steered party  $B$ , the steering party  $A$  becomes a reduced non-Gaussian state  $\rho_{B_a|A}$ . In some cases, we can generate Wigner negative states in the remote position.

For state  $\rho_j$ , we can derive its Wigner function by  $W_{\rho_j}(\gamma_j) = \text{Tr}(\hat{O}_{w_j} \rho_j)$ , with  $\hat{O}_{w_j} = \frac{2}{\pi} : e^{-2(\hat{a}_j^\dagger - \gamma_j^*)(\hat{a}_j - \gamma_j)} : (\dots : \text{denotes the normal ordering})$  and  $\gamma_j = (x_j + iy_j)/\sqrt{2}$ . Furthermore, we can quantify the WN of  $\rho_{B_a|A}$  as

$$\mathcal{N} \equiv \int |W(\gamma)| d^{2n_A} \gamma - 1, \quad (24)$$

with  $\gamma \in \mathbb{R}^{2n_A}$ , where  $n_A$  is the mode number considered in party  $A$ . As shown schematically in Fig.6, we propose protocols of generating 18 kinds of  $\rho_{B_a|A}$ s, whose analytical WFs are given in Appendix B. As examples, we plot

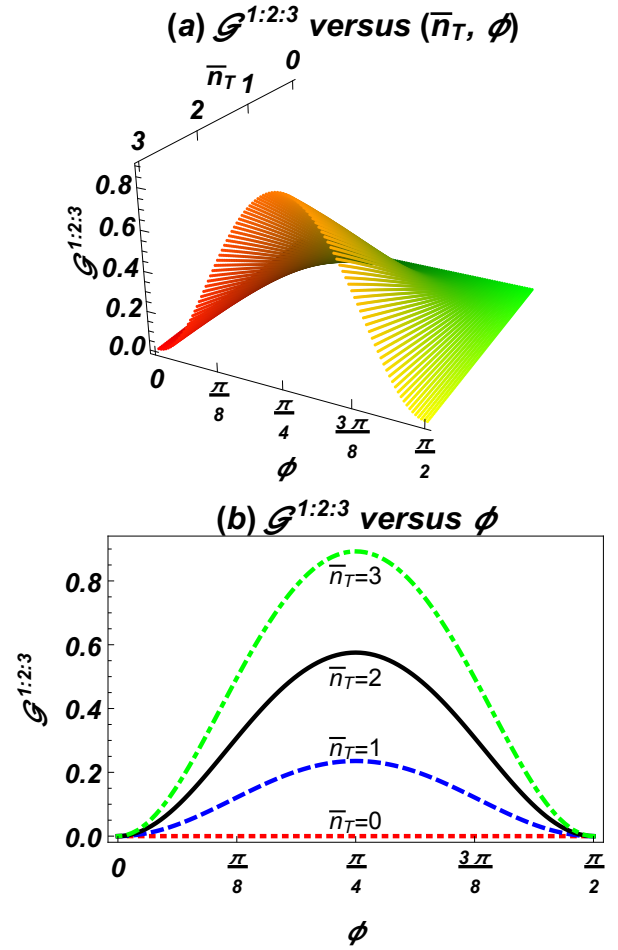


FIG. 5: RGS  $\mathcal{G}^{1:2:3}$  for the C3MSV with CM  $V$  (a) in the  $(\bar{n}_T, \phi)$  space; (b) versus  $\phi$  with different  $\bar{n}_T$ .

WFs for  $\rho_{B_a|A}$ s with  $\bar{n}_T = 3$  and  $\phi = \pi/8$  in Fig.7, where only several WFs exhibits the WNs.

Indeed, the amount of WN cannot be freely distributed among different modes. It can be influenced by the considered protocols and the interaction parameters. In order to explain the characters, we plot some WN  $\mathcal{N}$  versus  $\phi$  by fixing  $\bar{n}_T = 3$  in Fig.8 and versus  $\bar{n}_T$  by fixing  $\phi = \pi/8$  in Fig.9. The details are explained as follows.

*Case A(23)B(1):* In this case, the steering party  $A$  includes mode-2 and mode-3 and the steered party  $B$  includes mode-1. Performing appropriate photon subtraction(s) in the local position, we can remotely generate the following states with their respective WN

$$\begin{aligned} \rho_{1_a|23} &= \text{Tr}_1(\rho_{1_a23}) \rightarrow \mathcal{N}_{1_a|23}, \\ \rho_{1_a|2} &= \text{Tr}_{1,3}(\rho_{1_a23}) \rightarrow \mathcal{N}_{1_a|2}, \\ \rho_{1_a|3} &= \text{Tr}_{1,2}(\rho_{1_a23}) \rightarrow \mathcal{N}_{1_a|3}, \end{aligned} \quad (25)$$

where  $\rho_{1_a23} = |\epsilon_1|_1^{-2} \hat{a}_1 \rho_{123} \hat{a}_1^\dagger$ .

We plot  $\mathcal{N}_{1_a|23}$ ,  $\mathcal{N}_{1_a|2}$ , and  $\mathcal{N}_{1_a|3}$  as functions of  $\phi$  in Fig.8(a) and as functions of  $\bar{n}_T$  in Fig.9(a). From these figures, we find that WNs are generated remotely in the

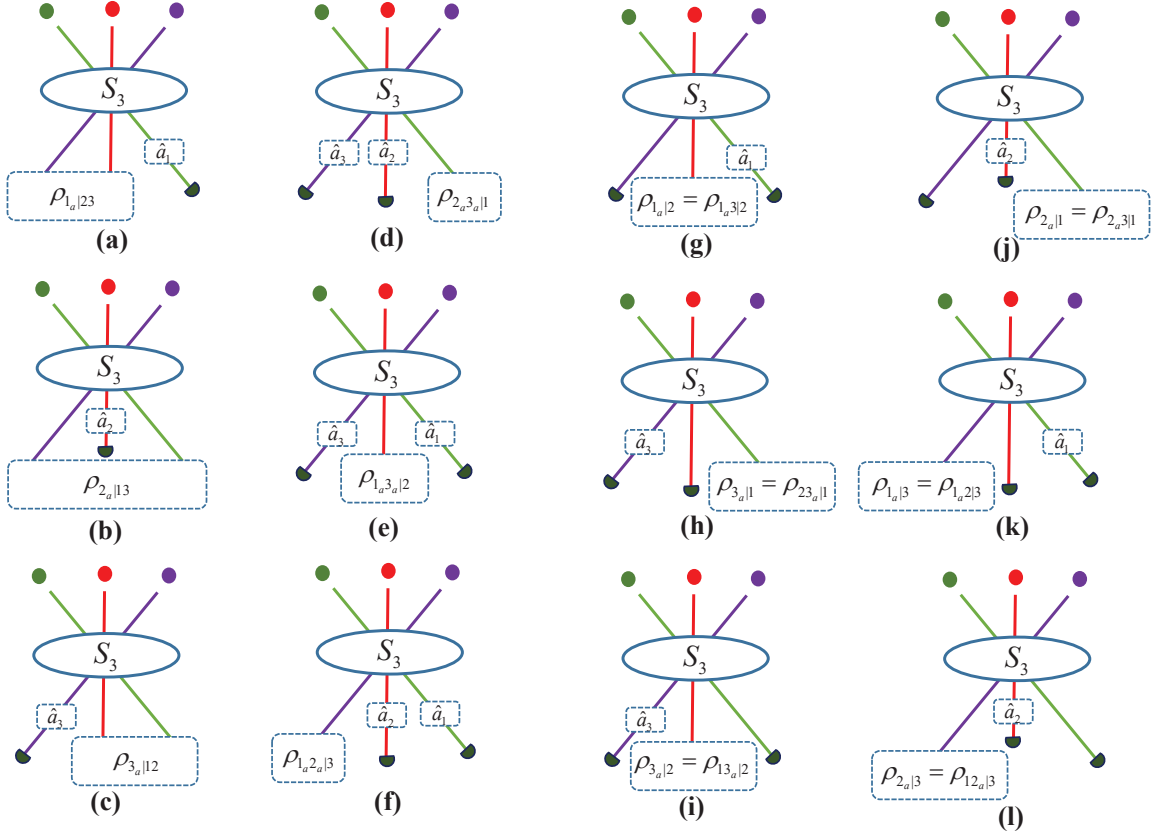


FIG. 6: Conceptual schemes of remote generated non-Gaussian states  $\rho_{B_a|A}$  based on the C3MSV. Note that Cases (a)-(c) are two-mode states and Cases (d)-(l) are one-mode states.

group (23), mode-2, mode-3, respectively, after a single-photon subtraction on mode-1. Moreover, we see that (1)  $\mathcal{N}_{1_a|23}$  is a monotonically increasing function of  $\phi$  from 0.04682 at  $\phi = 0$  to 0.42614 at  $\phi = \pi/2$ ; (2)  $\mathcal{N}_{1_a|2}$  remains as 0.04682 for any  $\phi$ ; (3)  $\mathcal{N}_{1_a|3}$  remains as 0 for any  $\phi$ ; (4)  $\mathcal{N}_{1_a|23} \geq \mathcal{N}_{1_a|2} + \mathcal{N}_{1_a|3}$ ; (5) As  $\bar{n}_T$  increasing, all these WNs will limit to 0.

*Case A(12)B(3):* In this case, the steering party  $A$  include mode-1 and mode-2 and the steered party  $B$  include mode-3. Performing appropriate photon subtraction(s) in the local position, we can remotely generate the following states with their respective WN

$$\begin{aligned} \rho_{3_a|12} &= \text{Tr}_3(\rho_{123_a}) \rightarrow \mathcal{N}_{3_a|12}, \\ \rho_{3_a|1} &= \text{Tr}_{2,3}(\rho_{123_a}) \rightarrow \mathcal{N}_{3_a|1}, \\ \rho_{3_a|2} &= \text{Tr}_{1,3}(\rho_{123_a}) \rightarrow \mathcal{N}_{3_a|2}, \end{aligned} \quad (26)$$

where  $\rho_{123_a} = |\epsilon_2|^{-2} \hat{a}_3 \rho_{123} \hat{a}_3^\dagger$ .

We plot  $\mathcal{N}_{3_a|12}$ ,  $\mathcal{N}_{3_a|1}$ , and  $\mathcal{N}_{3_a|2}$  as functions of  $\phi$  in Fig.8(b) and as functions of  $\bar{n}_T$  in Fig.9(b). From these figures, we find that WNs are generated remotely in the group (12), mode-1, mode-2, respectively, after a single-photon subtraction on mode-3. Moreover, we see that (1)  $\mathcal{N}_{3_a|12}$  is a monotonically decreasing function of  $\phi$  from 0.42614 at  $\phi = 0$  to 0.04682 at  $\phi = \pi/2$ ; (2)  $\mathcal{N}_{3_a|2}$

remains as 0.04682 for any  $\phi$ ; (3)  $\mathcal{N}_{3_a|1}$  remains as 0 for any  $\phi$ ; (4)  $\mathcal{N}_{3_a|12} \geq \mathcal{N}_{3_a|1} + \mathcal{N}_{3_a|2}$ ; (5) As  $\bar{n}_T$  increasing, all these WNs will limit to 0.

*Case A(13)B(2):* In this case, the steering party  $A$  includes mode-1 and mode-3 and the steered party  $B$  includes mode-2. Performing appropriate photon subtraction(s) in the local position, we can remotely generate the following states with their respective WN

$$\begin{aligned} \rho_{2_a|13} &= \text{Tr}_2(\rho_{12_a3}) \rightarrow \mathcal{N}_{2_a|13}, \\ \rho_{2_a|1} &= \text{Tr}_{2,3}(\rho_{12_a3}) \rightarrow \mathcal{N}_{2_a|1}, \\ \rho_{2_a|3} &= \text{Tr}_{1,2}(\rho_{12_a3}) \rightarrow \mathcal{N}_{2_a|3}, \end{aligned} \quad (27)$$

where  $\rho_{12_a3} = s^{-2} \hat{a}_2 \rho_{123} \hat{a}_2^\dagger$ .

We plot  $\mathcal{N}_{2_a|13}$ ,  $\mathcal{N}_{2_a|1}$ , and  $\mathcal{N}_{2_a|3}$  as functions of  $\phi$  in Fig.8(c) and as functions of  $\bar{n}_T$  in Fig.9(c). From these figures, we find that WNs are generated remotely in the group (13), mode-1, mode-3, respectively, after a single-photon subtraction on mode-2. Moreover, we see that (1)  $\mathcal{N}_{2_a|13}$  remains as 0.4683 for any  $\phi$ ; (2)  $\mathcal{N}_{2_a|1}$  decreases from 0.4683 to 0 in  $[0, \pi/4]$  and remains as 0 in  $[\pi/4, \pi/2]$ ; (3)  $\mathcal{N}_{2_a|3}$  remains as 0 in  $[0, \pi/4]$  and increases from 0 to 0.4683 in  $[\pi/4, \pi/2]$ ; (4)  $\mathcal{N}_{2_a|13} \geq \mathcal{N}_{2_a|1} + \mathcal{N}_{2_a|3}$ ; (5) As  $\bar{n}_T$  increasing, all these WNs will limit to 0.

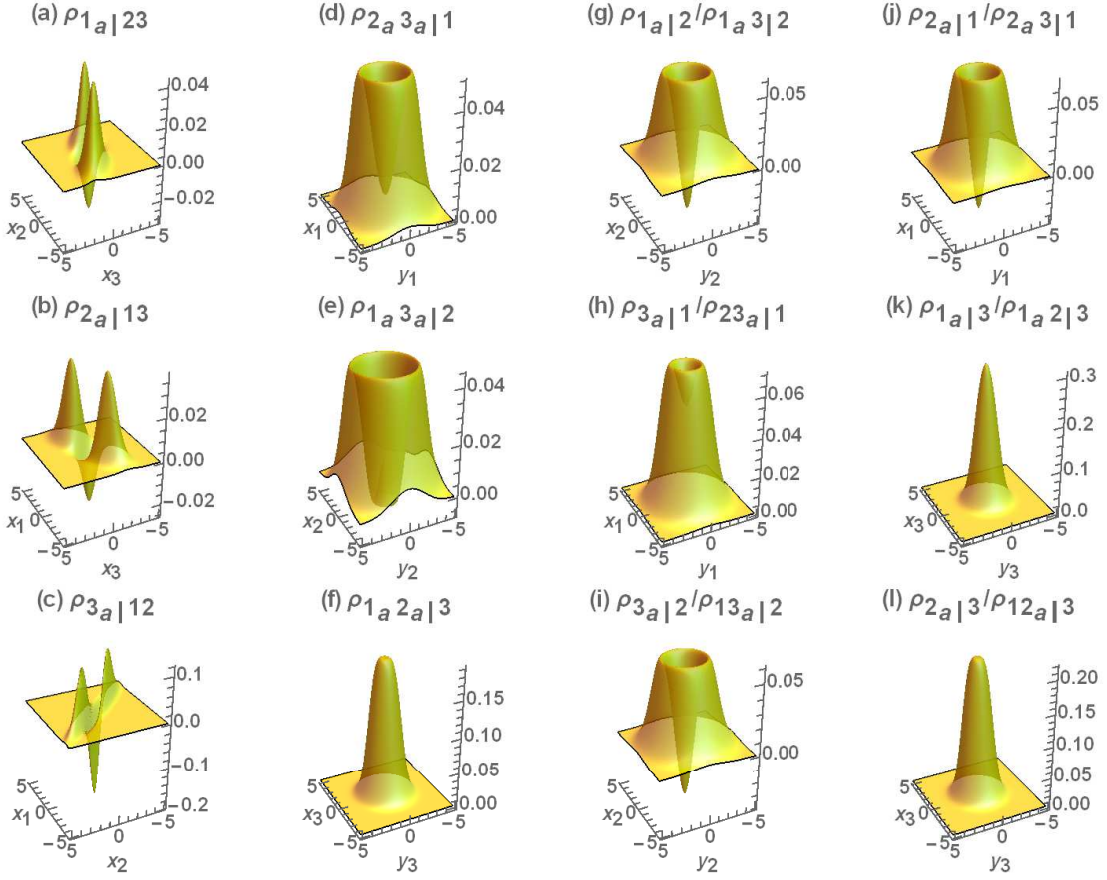


FIG. 7: WFs of  $\rho_{B_a|A S}$  corresponding to Fig.6, with  $\bar{n}_T = 3$ ,  $\phi = \pi/8$ , and  $\theta_1 = \theta_2 = 0$ . Some cases have WNs and some cases have no WNs.

*Case A(2)B(13):* In this case, the steering party  $A$  include mode-2 and the steered party  $B$  include mode-1 and mode-3. Performing appropriate photon subtraction(s) in the local position, we can remotely generate the following states with their respective WN

$$\begin{aligned} \rho_{1_a 3_a | 2} &= \text{Tr}_{1,3}(\rho_{1_a 23_a}) \rightarrow \mathcal{N}_{1_a 3_a | 2}, \\ \rho_{1_a 3 | 2} &= \text{Tr}_{1,3}(\rho_{1_a 23}) \rightarrow \mathcal{N}_{1_a 3 | 2}, \\ \rho_{13_a | 2} &= \text{Tr}_{1,3}(\rho_{123_a}) \rightarrow \mathcal{N}_{13_a | 2}, \end{aligned} \quad (28)$$

where  $\rho_{1_a 23_a} = \frac{1}{2} |\epsilon_1 \epsilon_2|^{-2} \hat{a}_1 \hat{a}_3 \rho_{123} \hat{a}_1^\dagger \hat{a}_3^\dagger$ .

We plot  $\mathcal{N}_{1_a 3_a | 2}$ ,  $\mathcal{N}_{1_a 3 | 2}$ , and  $\mathcal{N}_{13_a | 2}$  as functions of  $\phi$  in Fig.8(d) and as functions of  $\bar{n}_T$  in Fig.9(d). From these figures, we find that WNs are generated remotely in mode-2, after single-photon subtractions on each of the group (13), or a single-photon subtraction on mode-1 or mode-3, respectively. Here, we see that (1)  $\mathcal{N}_{1_a 3_a | 2}$  remains as 0.0318528, (2)  $\mathcal{N}_{1_a 3 | 2}$  and  $\mathcal{N}_{13_a | 2}$  remain as 0.04683; (3)  $\mathcal{N}_{1_a 3_a | 2} < \mathcal{N}_{1_a 3 | 2} + \mathcal{N}_{13_a | 2}$ ; (4) As  $\bar{n}_T$  increases, all these WNs will limit to 0. However, although  $\mathcal{G}^{2 \rightarrow 1} > 0$ ,  $\mathcal{G}^{2 \rightarrow 3} > 0$ , and  $\mathcal{G}^{2 \rightarrow (31)} > 0$ , we cannot achieve more significant increase of the WNs in mode-2, after performing a single-photon subtraction on each of mode-1 and mode-3.

*Case A(1)B(23):* In this case, the steering party  $A$  include mode-1 and the steered party  $B$  include mode-2 and mode-3. Performing appropriate photon subtraction(s) in the local position, we can remotely generate the following states with their respective WN

$$\begin{aligned} \rho_{2_a 3_a | 1} &= \text{Tr}_{2,3}(\rho_{12_a 3_a}) \rightarrow \mathcal{N}_{2_a 3_a | 1} \equiv 0, \\ \rho_{2_a 3 | 1} &= \text{Tr}_{2,3}(\rho_{12_a 3}) \rightarrow \mathcal{N}_{2_a 3 | 1} \equiv 0, \\ \rho_{23_a | 1} &= \text{Tr}_{2,3}(\rho_{123_a}) \rightarrow \mathcal{N}_{23_a | 1} \equiv 0, \end{aligned} \quad (29)$$

where  $\rho_{12_a 3_a} = (c^2 + s^2)^{-1} |\epsilon_2|^{-2} \hat{a}_2 \hat{a}_3 \rho_{123} \hat{a}_2^\dagger \hat{a}_3^\dagger$ . For any  $\bar{n}_T$  and  $\phi$ , we see  $\mathcal{N}_{2_a 3_a | 1} = \mathcal{N}_{2_a 3 | 1} = \mathcal{N}_{23_a | 1} \equiv 0$ . That is to say, no WNs are generated remotely in mode-1, after single-photon subtractions on each of the group (23), or a single-photon subtraction on mode-2, mode-3. Surprisingly,  $\mathcal{N}_{2_a 3_a | 1} = 0$  although  $\mathcal{G}^{1 \rightarrow 23} > 0$ .

*Case A(3)B(12):* In this case, the steering party  $A$  include mode-3 and the steered party  $B$  include mode-1 and mode-2. Performing appropriate photon subtraction(s) in the local position, we can remotely generate the following states with their respective WN

$$\begin{aligned} \rho_{1_a 2_a | 3} &= \text{Tr}_{1,2}(\rho_{1_a 2_a 3}) \rightarrow \mathcal{N}_{1_a 2_a | 3} \equiv 0, \\ \rho_{1_a 2 | 3} &= \text{Tr}_{1,2}(\rho_{1_a 23}) \rightarrow \mathcal{N}_{1_a 2 | 3} \equiv 0, \\ \rho_{12_a | 3} &= \text{Tr}_{1,2}(\rho_{12_a 3}) \rightarrow \mathcal{N}_{12_a | 3} \equiv 0, \end{aligned} \quad (30)$$

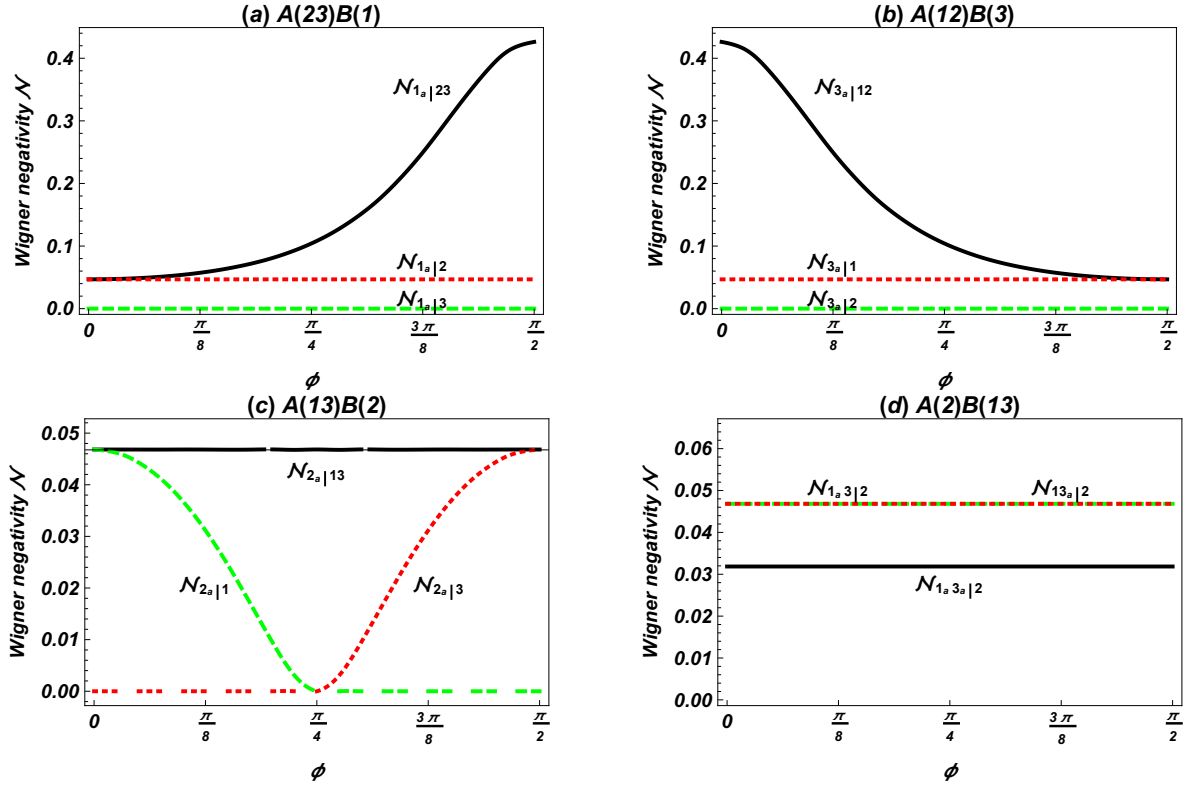


FIG. 8: WNs versus  $\phi$  with fixed  $\bar{n}_T = 3$ , for some  $\rho_{B_a|A}$ s in cases (a)  $A(23)B(1)$ , (b)  $A(12)B(3)$ , (c)  $A(13)B(2)$ , (d)  $A(2)B(13)$ .

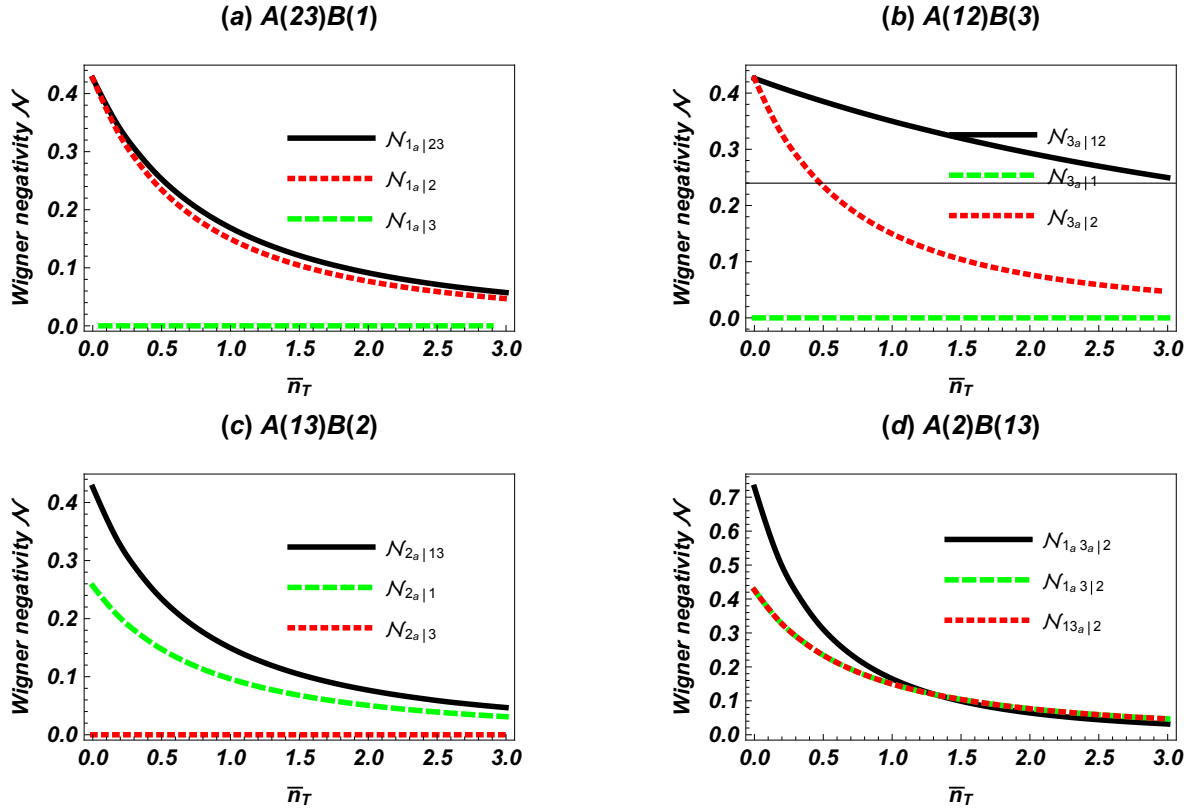


FIG. 9: WNs versus  $\bar{n}_T$  with fixed  $\phi = \pi/8$ , for some  $\rho_{B_a|A}$ s in cases (a)  $A(23)B(1)$ , (b)  $A(12)B(3)$ , (c)  $A(13)B(2)$ , (d)  $A(2)B(13)$ .

where  $\rho_{1_a 2_a 3} = (c^2 + s^2)^{-1} |\epsilon_1|^{-2} \hat{a}_1 \hat{a}_2 \rho_{123} \hat{a}_1^\dagger \hat{a}_2^\dagger$ . For any  $\bar{n}_T$  and  $\phi$ , we see  $\mathcal{N}_{1_a 2_a | 3} = \mathcal{N}_{1_a 2 | 3} = \mathcal{N}_{1_2 a | 3} \equiv 0$ . That is to say, no WNs are generated remotely in mode-3, after single-photon subtractions on each of the group (12), or a single-photon subtraction on mode-1, mode-2. Surprisingly,  $\mathcal{N}_{1_a 2_a | 3} = 0$  although  $\mathcal{G}^{3 \rightarrow 12} > 0$ .

## V. CONCLUSION

In this paper, we studied the steering property for the C3MSV and used the C3MSV as resource to generate Wigner-negative state. By taking different bipartite assignment in the C3MSV, we investigated all bipartite Gaussian steerings present in the C3MSV. These steerings include no seering, one-way steering and two-way steering. Moreover, the steerability can be adjusted by the interaction parameters. Using the C3MSV as the resource, we proposed schemes to remotely generate Wigner negative states. We analyzed and compared the distributions the Gaussian steering and the WNs over different modes.

Normally, if  $\mathcal{G}^{A \rightarrow B} > 0$ , then  $\mathcal{N} > 0$ ; if  $\mathcal{G}^{A \rightarrow B} = 0$ , then  $\mathcal{N} = 0$ . However, quantum correlations are not always a necessary requirement for the conditional generation of Wigner negativity[33]. For example, although  $\mathcal{G}^{1 \rightarrow 23} > 0$  and  $\mathcal{G}^{3 \rightarrow 12} > 0$ ,  $\rho_{2_a 3_a | 1}$  and  $\rho_{1_a 2_a | 3}$  cannot exhibit WN. Moreover, it is not always true that stronger steerability in the C3MSV induces more WNs.

We believe that the C3MSV will become an useful entangled resource in future quantum protocols. Its specific properties (including squeezing, entanglement and steering) has laid a good foundation for its applications in quantum technologies.

## Acknowledgments

This paper was supported by the National Natural Science Foundation of China (Grant No. 11665013).

## Appendix A: The C3MSO and the C3MSV

In this appendix, we give the transformation relation and the normal ordering form for the C3MSO. In addition, we give the general expression to calculate the expectation values we want for the C3MSV.

*About the C3MSO:* Using the formula of Bogoliubov transformation, we obtain the following transformation relations

$$S_3 A^\dagger S_3^\dagger = A^\dagger P^* + AL^*, S_3 A S_3^\dagger = AP + A^\dagger L, \quad (\text{A.1})$$

where  $A^\dagger = (\hat{a}_1^\dagger, \hat{a}_2^\dagger, \hat{a}_3^\dagger)$ ,  $A = (\hat{a}_1, \hat{a}_2, \hat{a}_3)$ , and

$$P = \begin{pmatrix} \kappa_1 & 0 & \tau \\ 0 & c & 0 \\ \tau^* & 0 & \kappa_2 \end{pmatrix}, L = \begin{pmatrix} 0 & \epsilon_1 & 0 \\ \epsilon_1 & 0 & \epsilon_2 \\ 0 & \epsilon_2 & 0 \end{pmatrix}. \quad (\text{A.2})$$

Here we set  $\kappa_1 = \sin^2 \phi + c \cos^2 \phi$ ,  $\kappa_2 = \cos^2 \phi + c \sin^2 \phi$ , and  $\tau = \frac{1}{2}(c-1)e^{i(\theta_2 - \theta_1)} \sin 2\phi$ .

According to the rule provided by Fan[52–54], we immediately obtain the normal ordering form of  $S_3$  as follows

$$S_3 = \frac{1}{\sqrt{\det P}} e^{-\frac{1}{2} A^\dagger (LP^{-1}) \bar{A}^\dagger} : e^{A^\dagger (\bar{P}^{-1} - I) \bar{A}} : e^{\frac{1}{2} A (P^{-1} L^*) \bar{A}}. \quad (\text{A.3})$$

Of course, we can further use  $: e^{A^\dagger (\bar{P}^{-1} - I) \bar{A}} := e^{A^\dagger (\ln \bar{P}^{-1}) \bar{A}}$  in above expression, where  $\bar{P}$  denotes the transpose of  $P$ .

*About the C3MSV:* Here, we give the following general expression

$$\begin{aligned} & \langle \hat{a}_1^{\dagger k_1} \hat{a}_2^{\dagger k_2} \hat{a}_3^{\dagger k_3} \hat{a}_1^{l_1} \hat{a}_2^{l_2} \hat{a}_3^{l_3} \rangle \\ &= \partial_{\mu_1}^{k_1} \partial_{\mu_2}^{k_2} \partial_{\mu_3}^{k_3} \partial_{\nu_1}^{l_1} \partial_{\nu_2}^{l_2} \partial_{\nu_3}^{l_3} \\ & e^{|\epsilon_1|^2 \mu_1 \nu_1 + s^2 \mu_2 \nu_2 + |\epsilon_2|^2 \mu_3 \nu_3 + \epsilon_1^* \epsilon_2 \mu_1 \nu_3 + \epsilon_1 \epsilon_2^* \mu_3 \nu_1} \\ & e^{-c \epsilon_1^* \mu_1 \mu_2 - c \epsilon_1 \nu_1 \nu_2 - c \epsilon_2^* \mu_2 \mu_3 - c \epsilon_2 \nu_2 \nu_3} \\ & |_{\mu_1 = \mu_2 = \mu_3 = \nu_1 = \nu_2 = \nu_3 = 0}, \end{aligned} \quad (\text{A.4})$$

from which one can study the statistical properties for the C3MSV.

## Appendix B: Wigner functions of remotely generated states

The WF for the C3MSV is

$$W_{\rho_{123}} = \frac{8}{\pi^3} e^{-2[(2\bar{n}_1 + 1)|\gamma_1|^2 + (2\bar{n}_2 + 1)|\gamma_2|^2 + (2\bar{n}_3 + 1)|\gamma_3|^2]} \times e^{-8[\text{Re}(c\epsilon_1^* \gamma_1 \gamma_2) + \text{Re}(\epsilon_1^* \epsilon_2 \gamma_1 \gamma_3^*) + \text{Re}(c\epsilon_2^* \gamma_2 \gamma_3)]}, \quad (\text{B.0})$$

which has the Gaussian form.

The analytical WFs of  $\rho_{B_a | A_s}$  are given as follows. For convenience of writing, we set  $\omega_0 = c^2 + s^2 = \cosh 2r$ ,  $\omega_1 = c^2 - s^2 \cos 2\phi$ ,  $\omega_2 = c^2 + s^2 \cos 2\phi$ . If  $\phi = 0$ , then  $\epsilon_2 = 0$ ,  $r = r_1$ ,  $\omega_1 = 1$  and  $\omega_2 = \omega_0$ ; If  $\phi = \pi/2$ , then  $\epsilon_1 = 0$ ,  $r = r_2$ ,  $\omega_1 = \omega_0$  and  $\omega_2 = 1$ .

(a) WF for  $\rho_{1_a | 23}$

$$W_{\rho_{1_a | 23}} = \frac{4e^{-2[|\omega_1| |\gamma_2|^2 + \omega_0 |\gamma_3|^2 + 4\text{Re}(c\epsilon_2^* \gamma_2 \gamma_3)]/\omega_2}}{\pi^2 \omega_3^3} \times (4|c\gamma_2 + \epsilon_2 \gamma_3^*|^2 - \omega_2). \quad (\text{B.1})$$

When  $\phi = 0$ , Eq.(B.1) will be reduced to  $W_{\rho_{1_a | 23}} = (2/\pi)e^{-2|\gamma_2|^2/\omega_0} (4c^2 \omega_0^{-3} |\gamma_2|^2 - \omega_0^{-2}) \times (2/\pi)e^{-2|\gamma_3|^2}$ .

(b) WF for  $\rho_{2_a | 13}$

$$W_{\rho_{2_a | 13}} = \frac{4e^{-2[|\omega_1| |\gamma_1|^2 + \omega_2 |\gamma_3|^2 - 4\text{Re}(\epsilon_1^* \epsilon_2 \gamma_1 \gamma_3^*)]/\omega_0}}{\pi^2 s^2 \omega_3^3} \times (4c^2 |\epsilon_1^* \gamma_1 + \epsilon_2^* \gamma_3|^2 - \omega_0 s^2). \quad (\text{B.2})$$

When  $\phi = 0$ , Eq.(B.3) will be reduced to  $W_{\rho_{2a|13}} = (2/\pi)e^{-2|\gamma_1|^2/\omega_0}(4c^2\omega_0^{-3}\cos^2\phi|\gamma_1|^2 - \omega_0^{-2}) \times (2/\pi)e^{-2|\gamma_3|^2}$ ; When  $\phi = \pi/2$ , Eq.(B.3) will be reduced to  $W_{\rho_{2a|13}} = (2/\pi)e^{-2|\gamma_3|^2/\omega_0}(4c^2\omega_0^{-3}\sin^2\phi|\gamma_3|^2 - \omega_0^{-2}) \times (2/\pi)e^{-2|\gamma_1|^2}$ .

(c) WF for  $\rho_{3a|12}$

$$W_{\rho_{3a|12}} = \frac{4e^{-2[\omega_2|\gamma_2|^2 + \omega_0|\gamma_1|^2 + 4\text{Re}(c\epsilon_1^*\gamma_1\gamma_2)]}/\omega_1}{\pi^2\omega_1^3} \times (4|c\gamma_2 + \epsilon_1\gamma_1^*|^2 - \omega_1). \quad (\text{B.3})$$

When  $\phi = \pi/2$ , Eq.(B.2) will be reduced to  $W_{\rho_{3a|12}} = (2/\pi)e^{-2|\gamma_2|^2/\omega_0}(4c^2\omega_0^{-3}|\gamma_2|^2 - \omega_0^{-2}) \times (2/\pi)e^{-2|\gamma_1|^2}$ .

(d) WF for  $\rho_{2a3a|1}$

$$W_{\rho_{2a3a|1}} = \frac{2e^{-2|\gamma_1|^2/\omega_2}}{\pi\omega_0\omega_2^5} \times [\omega_2^2\omega_1 + 4|\epsilon_1\gamma_1|^2(4c^4 + 4c^2|\epsilon_1\gamma_1|^2 - \omega_1^2)] \quad (\text{B.4})$$

When  $\phi = \pi/2$ , Eq.(B.4) will be reduced to  $W_{\rho_{2a3a|1}} = (2/\pi)e^{-2|\gamma_1|^2}$ .

(e) WF for  $\rho_{1a3a|2}$

$$W_{\rho_{1a3a|2}} = \frac{2e^{-2|\gamma_2|^2/\omega_0}}{\pi\omega_0^5}(\omega_0^2 + 8c^4|\gamma_2|^4 - 8\omega_0c^2|\gamma_2|^2), \quad (\text{B.5})$$

which is independent of  $\phi$ .

(f) WF for  $\rho_{1a2a|3}$

$$W_{\rho_{1a2a|3}} = \frac{2e^{-2|\gamma_3|^2/\omega_1}}{\pi\omega_0\omega_1^5} \times [\omega_1^2\omega_2 + 4|\epsilon_2\gamma_3|^2(4c^4 + 4c^2|\epsilon_2\gamma_3|^2 - \omega_2^2)]. \quad (\text{B.6})$$

When  $\phi = 0$ , Eq.(B.6) will be reduced to  $W_{\rho_{1a2a|3}} = (2/\pi)e^{-2|\gamma_3|^2}$ .

(g) WF for  $\rho_{1a|2}$  and  $\rho_{1a3|2}$

$$W_{\rho_{1a|2}} = W_{\rho_{1a3|2}} = \frac{2e^{-2|\gamma_2|^2/\omega_0}}{\pi\omega_0^3}(4c^2|\gamma_2|^2 - \omega_0), \quad (\text{B.7})$$

which is independent of  $\phi$ .

(h) WF for  $\rho_{3a|1}$  and  $\rho_{23a|1}$

$$W_{\rho_{3a|1}} = W_{\rho_{23a|1}} = \frac{2e^{-2|\gamma_1|^2/\omega_2}}{\pi\omega_2^3}(4|\epsilon_1\gamma_1|^2 + \omega_2). \quad (\text{B.8})$$

When  $\phi = \pi/2$ , Eq.(B.8) will be reduced to  $W_{\rho_{3a|1}} =$

$W_{\rho_{23a|1}} = (2/\pi)e^{-2|\gamma_1|^2}$ .

(i) WF for  $\rho_{3a|2}$  and  $\rho_{13a|2}$

$$W_{\rho_{3a|2}} = W_{\rho_{13a|2}} = \frac{2e^{-2|\gamma_2|^2/\omega_0}}{\pi\omega_0^3}(4c^2|\gamma_2|^2 - \omega_0), \quad (\text{B.9})$$

which is independent of  $\phi$ .

(j) WF for  $\rho_{2a|1}$  and  $\rho_{2a3|1}$

$$W_{\rho_{2a|1}} = W_{\rho_{2a3|1}} = \frac{2e^{-2|\gamma_1|^2/\omega_2}}{\pi\omega_2^3}(4c^2|\gamma_1|^2\cos^2\phi - \omega_2\cos 2\phi). \quad (\text{B.10})$$

When  $\phi = \pi/2$ , Eq.(B.10) will be reduced to  $W_{\rho_{2a|1}} =$

$W_{\rho_{2a3|1}} = (2/\pi)e^{-2|\gamma_1|^2}$ .

(k) WF for  $\rho_{1a|3}$  and  $\rho_{1a2|3}$

$$W_{\rho_{1a|3}} = W_{\rho_{1a2|3}} = \frac{2e^{-2|\gamma_3|^2/\omega_1}}{\pi\omega_1^3}(4|\epsilon_2\gamma_3|^2 + \omega_1). \quad (\text{B.11})$$

When  $\phi = 0$ , Eq.(B.11) will be reduced to  $W_{\rho_{1a|3}} =$

$W_{\rho_{1a2|3}} = (2/\pi)e^{-2|\gamma_3|^2}$ .

(l) WF for  $\rho_{2a|3}$  and  $\rho_{12a|3}$

$$W_{\rho_{2a|3}} = W_{\rho_{12a|3}} = \frac{2e^{-2|\gamma_3|^2/\omega_1}}{\pi\omega_1^3}(4c^2|\gamma_3|^2\sin^2\phi + \omega_1\cos 2\phi). \quad (\text{B.12})$$

When  $\phi = 0$ , Eq.(B.12) will be reduced to  $W_{\rho_{2a|3}} =$

$W_{\rho_{12a|3}} = (2/\pi)e^{-2|\gamma_3|^2}$ .

- 
- [1] R. Horodecki, P. Horodecki, M. Horodecki, and K. Horodecki, Quantum entanglement, *Rev. Mod. Phys.* **81**, 865 (2009).
- [2] A. N. Boto, P. Kok, D. S. Abrams, S. L. Braunstein, C. P. Williams, and J. P. Dowling, Quantum Interferometric Optical Lithography: Exploiting Entanglement to Beat the Diffraction Limit, *Phys. Rev. Lett.* **85**, 2733 (2000).
- [3] N. Mohseni, S. Saeidian, J. P. Dowling, and C. Navarrete-Benlloch, Deterministic generation of hybrid high-N NOON states with Rydberg atoms trapped in microwave cavities, *Phys. Rev. A* **101**, 013804 (2020).

- [4] Greenberger, D. M., M. A. Horne, and A. Zeilinger, *Going Beyond Bell's Theorem in Bell's Theorem, Quantum Theory, and Conceptions* (the Universe Kluwer Academic, Dordrecht, 1989).
- [5] T. Aoki, N. Takei, H. Yonezawa, K. Wakui, T. Hiraoka, and A. Furusawa, Experimental Creation of a Fully Inseparable Tripartite Continuous-Variable State, *Phys. Rev. Lett.* **91**, 080404 (2003).
- [6] P. van Loock and Samuel L. Braunstein, Multiparticle Entanglement for Continuous Variables: A Quantum Teleportation Network, *Phys. Rev. Lett.* **84**, 3482 (2000).

- [7] E. A. Rojas Gonzalez, A. Borne, B. Boulanger, J. A. Levenson, and K. Bencheikh, Continuous-Variable Triple-Photon States Quantum Entanglement, *Phys. Rev. Lett.* **120**, 043601 (2018).
- [8] S. B. Xie and J. H. Eberly, Triangle Measure of Tripartite Entanglement, *Phys. Rev. Lett.* **127**, 040403 (2021).
- [9] A. Suprano, D. Poderini, E. Polino, I. Agresti, G. Carvacho, A. Canabarro, E. Wolfe, R. Chaves, and F. Sciarrino, Experimental Genuine Tripartite Nonlocality in a Quantum Triangle Network, *PRX QUANTUM* **3**, 030342 (2022).
- [10] W. Zhang and R. T. Glasser, Coupled Three-Mode Squeezed Vacuum, arXiv: 2002.00323 (2022).
- [11] K. Modi, A. Brodutch, H. Cable, T. Paterek, and Vedral, The classical-quantum boundary for correlations: Discord and related measures, *Rev. Mod. Phys.* **84**, 1655 (2012).
- [12] L. M. Duan, G. Giedke, J. I. Cirac, and P. Zoller, Inseparability Criterion for Continuous Variable Systems, *Phys. Rev. Lett.* **84**, 2722 (2000).
- [13] J. S. Bell, On the Einstein podolsky rosen paradox, *Physics* **1**, 195 (1964).
- [14] N. Brunner, D. Cavalcanti, S. Pironio, V. Scarani, and S. Wehner, Bell nonlocality, *Phys. Mod. Phys.* **86**, 419 (2014).
- [15] V. Scarani, *Bell Nonlocality* (Oxford University Press, 2019).
- [16] I. Kogias, A. R. Lee, S. Ragy, and G. Adesso, Quantification of Gaussian Quantum Steering, *Phys. Rev. Lett.* **114**, 060403 (2015).
- [17] P. Skrzypczyk, M. Navascues, and D. Cavalcanti, Quantifying Einstein-Podolsky-Rosen Steering, *Phys. Rev. Lett.* **112**, 180404 (2014).
- [18] Q. Y. He, Q. H. Gong, and M. D. Reid, Classifying Directional Gaussian Entanglement, Einstein-Podolsky-Rosen Steering, and Discord, *Phys. Rev. Lett.* **114**, 060402 (2015).
- [19] S. Armstrong, M. Wang, R. Y. Teh, Q. H. Gong, Q. Y. He, J. Janousek, H. A. Bachor, M. D. Reid, and P. K. Lam, Multipartite Einstein-Podolsky-Rosen steering and genuine tripartite entanglement with optical networks, *Nat. Phys.* **11**, 167 (2015).
- [20] Q. Y. He and M. D. Reid, Genuine Multipartite Einstein-Podolsky-Rosen Steering, *Phys. Rev. Lett.* **111**, 250403 (2013).
- [21] H. M. Wiseman, S. J. Jones, and A. C. Doherty, Steering, Entanglement, Nonlocality, and the Einstein-Podolsky-Rosen Paradox, *Phys. Rev. Lett.* **98**, 140402 (2007).
- [22] S. J. Jones, H. M. Wiseman, and A. C. Doherty, Entanglement, Einstein-Podolsky-Rosen correlations, Bell nonlocality, and steering, *Phys. Rev. A* **76**, 052116 (2007).
- [23] C. H. Bennett, G. Brassard, C. Crepeau, R. Jozsa, A. Peres, and W. K. Wootters, *Phys. Rev. Lett.* **70**, 1895 (1993).
- [24] R. Horodecki, P. Horodecki, M. Horodecki, and K. Horodecki, Quantum entanglement, *Rev. Mod. Phys.* **81**, 865 (2009).
- [25] M. D. Reid, P. D. Drummond, W. P. Bowen, E. G. Cavalcanti, P. K. Lam, H. A. Bachor, U. L. Andersen, and G. Leuchs, The Einstein-Podolsky-Rosen paradox: From concepts to applications, *Rev. Mod. Phys.* **81**, 1727 (2009).
- [26] R. Uola, A. C. S. Costa, H. Chau Nguyen, and O. Gühne, Quantum steering, *Rev. Mod. Phys.* **92**, 015001 (2020).
- [27] A. Kenfack and K. Życzkowski, Negativity of the Wigner function as an indicator of non-classicality, *J. Opt. B: Quantum Semiclass. Opt.* **6**, 396 (2004).
- [28] U. Chabaud, P. E. Emeriau, F. Grosshans, Witnessing Wigner Negativity, *Quantum* **5**, 471 (2021).
- [29] F. Albarelli, M. G. Genoni, M. G. A. Paris, and A. Ferraro, Resource theory of quantum non-Gaussianity and Wigner negativity, *Phys. Rev. A* **98**, 052350 (2018).
- [30] R. Takagi and Q. Zhuang, Convex resource theory of non-Gaussianity, *Phys. Rev. A* **97**, 062337 (2018).
- [31] A. Mari and J. Eisert, Positive Wigner Functions Render Classical Simulation of Quantum Computation Efficient, *Phys. Rev. Lett.* **109**, 230503 (2012).
- [32] S. Rahimi-Keshari, T. C. Ralph, and C. M. Caves, Sufficient Conditions for Efficient Classical Simulation of Quantum Optics, *Phys. Rev. X* **6**, 021039 (2016).
- [33] M. Walschaers, On Quantum Steering and Wigner Negativity, arXiv: 2211.14102 (2022).
- [34] M. Walschaers, C. Fabre, V. Parigi, and N. Treps, Entanglement and Wigner function negativity of multimode non-Gaussian states, *Phys. Rev. Lett.* **119**, 183601 (2017).
- [35] M. Walschaers and N. Treps, Remote Generation of Wigner Negativity through Einstein-Podolsky-Rosen Steering, *Phys. Rev. Lett.* **124**, 150501 (2020).
- [36] M. Walschaers, V. Parigi, and N. Treps, Practical Framework for Conditional Non-Gaussian Quantum State Preparation, *PRX Quantum* **1**, 020305 (2020).
- [37] M. Walschaers, Non-Gaussian Quantum States and Where to Find Them, *PRX Quantum* **2**, 030204 (2021).
- [38] Y. Xiang, S. H. Liu, J. J. Guo, Q. H. Gong, N. Treps, Q. Y. He and M. Walschaers, Distribution and quantification of remotely generated Wigner negativity, *npj Quantum Information* **8**, 21 (2022).
- [39] R. W. Boyd, *Nonlinear Optics* (Academic Press, Third Edition, 2008).
- [40] M. O. Scully and M. S. Zubairy, *Quantum Optics* (Cambridge University Press, 1997).
- [41] A. Serafini, *Quantum Continuous Variables: A Primer of Theoretical Methods* (CRC Press, 2017).
- [42] M. G. Genoni, L. Lami, and A. Serafini, Conditional and unconditional gaussian quantum dynamics. *Contem. Phys.*, **57**, 331 (2016).
- [43] C. Weedbrook, S. Pirandola, R. Garcia-Patron, N. J. Cerf, T. C. Ralph, J. H. Shapiro, and S. Lloyd, Gaussian quantum information, *Rev. Mod. Phys.* **84**, 621 (2012).
- [44] J. B. Brask, Gaussian states and operations - a quick reference, arXiv: 2102.05748 (2021).
- [45] I. Brandao, D. Tandeitnik, and T. Guerreiro, QuGIT: a numerical toolbox for Gaussian quantum states, *Computer Physics Communications* **280**, 108471 (2022).
- [46] L. Lami, C. Hirche, G. Adesso, and A. Winter, Schur Complement Inequalities for Covariance Matrices and Monogamy of Quantum Correlations, *Phys. Rev. Lett.* **117**, 220502 (2016).
- [47] M. Frigerio, C. Destri, S. Olivares, M. G. A. Paris, Quantum steering with Gaussian states: A tutorial, *Phys. Lett. A* **430**, 127954 (2022).
- [48] M. D. Reid, Monogamy inequalities for the Einstein-Podolsky-Rosen paradox and quantum steering, *Phys. Rev. A* **88**, 062108 (2013).
- [49] Y. Xiang, I. Kogias, G. Adesso, and Q. Y. He, Multipartite Gaussian steering: Monogamy constraints and quantum cryptography applications, *Phys. Rev. A* **95**, 010101(R) (2017).
- [50] I. Kogias, A. R. Lee, S. Ragy, and G. Adesso, Quantification of Gaussian Quantum Steering, *Phys. Rev. Lett.* **114**, 060403 (2015).
- [51] Y. Xiang, S. M. Cheng, Q. H. Gong, Z. Ficek, and Q. Y.

- He, Quantum Steering: Practical Challenges and Future Directions, *PRX Quantum* **3**, 030102 (2022).
- [52] H. Y. Fan, Normally ordering some multimode exponential operators by virtue of the IWOP technique, *J. Phys. A: Math. Gen.* **23**, 1833 (1990).
- [53] H. Y. Fan and H. Zou, Similarity transformation operators as the images of classical symplectic transformations in coherent state representation, *Phys. Lett. A* **252**, 281 (1999).
- [54] H. Y. Fan and J. VanderLinde, Similarity transformations in one- and two-mode Fock space, *J. Phys. A: Math. Gen.* **24**, 2529 (1991).